DOI: 10.1002/cvde.201507190

# A Process-Structure Investigation of Aluminum Oxide and Oxycarbide Thin Films prepared by Direct Liquid Injection CVD of Dimethylaluminum Isopropoxide (DMAI)**

By *Loïc Baggetto*, Cédric Charvillat, Jérôme Esvan, Yannick Thébault, Diane Samélor, Hugues Vergnes, Brigitte Caussat, Alain Gleizes,* and *Constantin Vahlas**

We present the direct liquid injection CVD of aluminum oxide and oxycarbide thin films using dimethylaluminum isopropoxide at high process temperature (500–700 °C) with the addition of $O_2$ gas, and at low temperature (150–300 °C) with the addition of $H_2O$ vapor. Very smooth films with typical roughness values lower than 2 nm are obtained. The thin films are composed of an amorphous material. The composition evolves as a function of temperature from that of a partial hydroxide to a stoichiometric oxide at low deposition temperature (150–300 °C), and from that of a stoichiometric oxide to a mixture of an oxide with an (oxy) carbide at higher temperature (500–700 °C).

Keywords: Aluminum tri-isopropoxide, Amorphous aluminum oxide and oxycarbide film, Dimethylaluminum isopropoxide, Direct liquid injection, MOCVD

## 1. Introduction

Aluminum oxide is a material of major technological interest for a wide range of applications in optical and microelectronic components. Alumina is also widely used as a wear resistance agent and catalyst support, and as a corrosion and thermal oxidation barrier.[1–3] The protection from corrosion and thermal oxidation of composite polymer materials, light alloys (Ti- and Mg-based), and stainless steels used in aeronautic and automotive applications calls for the development of alumina films with superior performances for moderate temperature applications (200–600 °C).[4,5] Overall, the number of reports on the preparation of alumina films is significant using either physical vapor deposition (PVD) or CVD techniques. A practical way to produce amorphous alumina films onto complex-in-shape substrates is metal-organic (MO) CVD,[4–9] in which a controlled amount of metal-organic precursor carried over a surface decomposes and reacts to form a conformal condensate thin layer.

Aluminum tri-isopropoxide (ATI) is a CVD precursor with significant advantages since it is stable in air, only slowly reactive with water, and it is cheap; however the oligomerization, decomposition, and subsequent condensation of sub-products, due to thermal ageing, pose problems,[10] and lead to worsening film properties as well as tedious reactor maintenance due to line pollution and injector blockage. Furthermore, the applicable range of deposition temperature used with ATI is not only limited by the stability window of the substrate, but is also constrained by the microstructure and elemental composition of the obtained film. Indeed, amorphous alumina films grown from evaporated ATI are hydroxylated for temperatures below 480 °C, and have optimal mechanical, corrosion, and oxidation protection properties around 500–550 °C.[10–12]

Trimethylaluminum (TMA) was also evaluated as a CVD precursor to form alumina films. In addition to an oxidizing agent, however, the process can require the use of a catalytic support (Ir, Ni-Cr alloys) or plasma assistance,[13] and otherwise employs deposition temperatures equal to, or higher than, those employed for ATI.[14] These relatively high temperatures may limit the use of TMA- and ATI-processed alumina films for the protection of materials for which the properties, e.g., mechanical, change significantly above 200–300 °C. This is the case, for instance, of Mg alloys and polymer composites. Dimethylaluminum isopropoxide (DMAI) was proposed by a few groups as an alternative CVD precursor to produce alumina films using evaporation or bubbling systems.[7,8,15–20] DMAI was also tested for

[*] Dr. L. Baggetto, C. Charvillat, J. Esvan, Y. Thébault, D. Samélor, Prof. A. Gleizes, Dr. C. Vahlas
Centre Inter-universitaire de Recherche et d'Ingéniérie des Matériaux (CIRIMAT), UMR5085 CNRS, 4 allée Emile Monso, BP-44362, 31030 Toulouse Cedex 4, France
E-mail: loic.baggetto@ensiacet.fr; constantin.vahlas@ensiacet.fr
Dr. H. Vergnes, Prof. B. Caussat
Laboratoire de Génie Chimique (LGC), Université de Toulouse, 4 allée Emile Monso, CS-84234, 31432 Toulouse Cedex 4, France

[**] Philippe de Parseval (UMS3623, CNRS) is gratefully acknowledged for conducting EPMA measurements. Christophe Capello is gratefully acknowledged for carrying out the sawing of Si substrates. This work was financially supported by the STAE-RTRA foundation (Toulouse, France) under the RTRA-STAE/2014/P/VIMA/12 project grant.

atomic layer deposition (ALD) of alumina in a few instances.[21–24] This molecule consists of an Al atom linked to two methyl and one isopropyl groups, and has an intermediate structure between ATI and TMA. Unlike TMA, the remaining isopropyl group in DMAI stabilizes the molecule which is non pyrophoric. Moreover, even though the presence of two Al-$CH_3$ bonds in DMAI makes it very reactive with water, the molecule presents a significantly higher vapor pressure than ATI, it is liquid at room temperature, has a longer shelf-life, and is not prone to oligomerization. There has been a report on the growth of amorphous alumina films from DMAI in the presence of water vapor between 180 and 270 °C,[8] this temperature range being significantly lower than that of ATI processes. Such low deposition temperature paves the way for the protection of light alloys or polymer composite materials using amorphous alumina.

Although less investigated and less frequently used, aluminum oxycarbides, possibly derived from DMAI precursor, also present significant technological interests, mainly due to their excellent mechanical properties. It has been reported, for example, that the strength, hardness, and fracture toughness of hot-pressed SiC-$Al_2OC$ ceramics ($\sigma_f = 660$ MPa, $H = 27.1$ GPa, $K_{Ic} = 3.1$ MPa $m^{1/2}$, respectively) are comparable with, or superior to, the corresponding properties of commercial grades of sintered SiC.[25] On the other hand, processing of aluminum oxycarbides such as $Al_4O_4C$ or $Al_2OC$ often proceeds at high temperature and has never been reported in the form of thin films.

We have recently reported, for the first time, the development of such CVD processes involving the direct liquid injection (DLI) of DMAI diluted in cyclohexane.[26] The present contribution further consolidates these results by comparing them with the results for films obtained by the evaporation of ATI. The advantages of DMAI, combined with the use of a DLI system instead of a bubbler technology for the transport of the precursor in the deposition area make the DLI of DMAI an a-priori interesting alternative to evaporated ATI in CVD processes. Indeed, the injection system offers several advantages over classic sublimation and evaporation techniques since it provides constant precursor vapor flow and leads to a more stable, robust, and reproducible process.[27] Two oxygenating atmospheres were employed, as selected from former works using the aforementioned classic systems.[7,8,15–20] Battiston and co-workers reported the fabrication of stoichiometric and carbon-free alumina films using $O_2$ and $H_2O$ oxygenating atmospheres,[7,8] whereas other authors consistently measured carbon leftovers in their films when using pure $N_2$.[17–19] Here, at high deposition temperatures (>500 °C), a $N_2/O_2$ mixture was used to compensate for the lower than 1.5 O/Al ratio in DMAI, and to possibly prevent the incorporation of carbon in the films. At lower deposition temperatures (<300 °C), a $N_2/H_2O$ mixture was used to compensate for the lack of oxygen in DMAI while promoting the reaction kinetics. The physico-chemical properties of our thin films were characterized using a wide set of techniques. Results regarding the morphology and composition were compared to those obtained for alumina films produced by the evaporation of ATI. Surface morphology and roughness were measured using scanning electron microscopy (SEM) and atomic force microscopy (AFM). The amorphous state of the films was ascertained by X-ray diffraction (XRD). Elemental compositions, as well as the chemical environments of the bulk of the film, with emphasis on the formation of partial hydroxyls or (oxy) carbides, were determined through X-ray photoelectron spectroscopy (XPS) and electron probe microanalysis (EPMA).

## 2. Results and Discussion

The surface morphology and roughness measured by AFM for a film grown at 520 °C from evaporated ATI, and for two films grown at 200 °C from DMAI in the presence of $H_2O$ and at 600 °C from DMAI in the presence of $O_2$, are shown in Figure 1. The corresponding roughness parameters are listed in Table 1. The film surfaces are composed of a large density of peaks with varying shapes, heights, and lateral widths. Overall, it appears that the density and height of the peaks increases with deposition temperature, while the lateral widths decrease with increasing temperature. The film grown from evaporated ATI at 520 °C (Fig. 1a) has arithmetic and root mean square (rms) roughness values of 4.79 and 6.09 nm, respectively, while the two films obtained from the DMAI precursor are significantly smoother (Fig. 1b and Fig. 1c), with typical roughness values between 0.90 and 1.25 nm for the film grown at 200 °C in the presence of $H_2O$, and between 1.30 and 1.75 nm for the film grown at 600 °C in the presence of $O_2$. These results suggest faster surface diffusion and/or higher nuclei density for the growth of alumina from DMAI precursor. In all cases, the relatively low roughness and absence of nodules support the absence of homogeneous gas-phase reactions. Moreover, the low roughness values suggest the formation of a high density of nucleation centers during the film deposition, as was proposed to explain the smoothness of alumina films prepared at low temperatures (180–270 °C) using evaporated DMAI.[8] The results obtained here at high temperatures contrast with those reported for alumina films prepared between 540 and 600 °C by the evaporation of DMAI for which significantly rougher films were obtained.[7] This difference might result from the lower deposition rate used in our work (Table 2), which gives surface diffusion and atomic rearrangement more time to take place.

The sample cross-sections imaged by SEM are shown in Figure 2. In agreement with AFM observations, the films are extremely smooth, do not show any pinholes and look dense. It is interesting to note that the material obtained from evaporated ATI at 520 °C (Fig. 2a) shows a

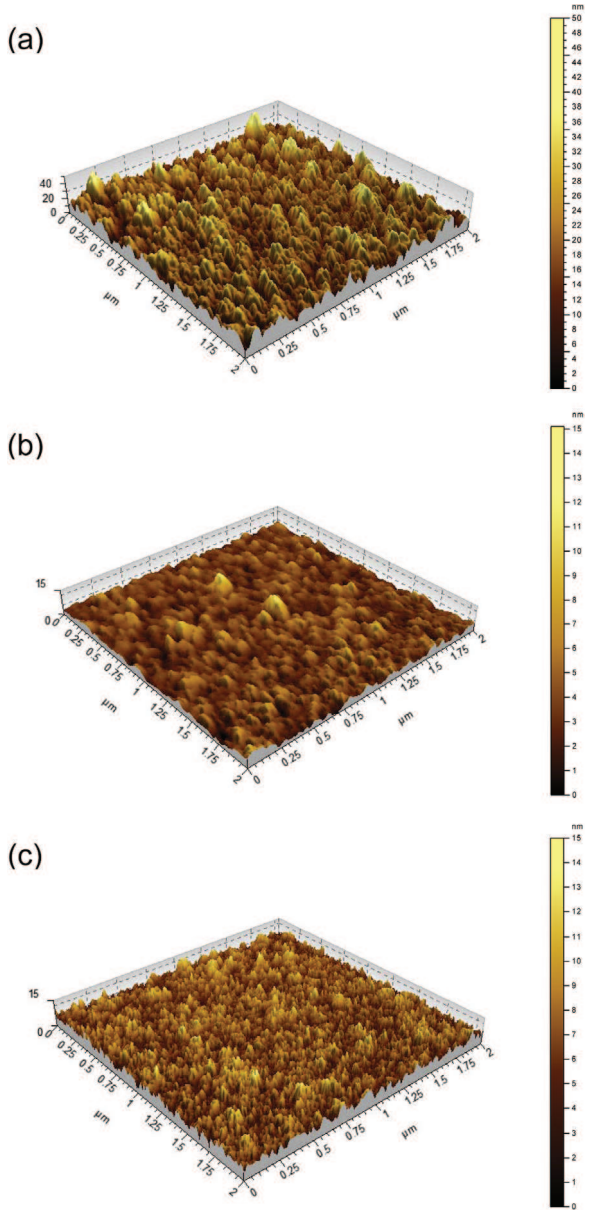


Fig. 1. 3D topography images of the surfaces measured by contact AFM for alumina films deposited onto Si substrates using a) evaporated ATI in $N_2$ at 520 °C, and for films grown by DLI CVD of DMAI, b) at 200 °C in the presence of $H_2O$, and c) at 600 °C in the presence of $O_2$. The roughness parameters derived from the measurements are listed in Table 1. Note the differences in height scale bars.

cross-section microstructure similar to that of the material obtained with the DLI CVD of DMAI at 600 °C in the presence of $O_2$, which could be related to the similar deposition temperatures. The measurement of the film thickness (see Fig. 2 caption) in the cross-section views was found to be in very good agreement with the optical reflectivity measurements, with maximum deviations of about 5%.

The amorphous structure of the thin film materials obtained from a DMAI precursor was ascertained by XRD

Table 1. Roughness parameters [nm] of alumina films prepared from DMAI at 200 °C in the presence of $H_2O$ and at 600 °C in the presence of $O_2$ (Fig. 1), and for films grown using evaporated ATI at 520 °C. Values are obtained by contact mode AFM measurements over a 2 μm × 2 μm area. $S_a$ and $S_q$ stand for the areal arithmetic and rms roughness, respectively of an entire area scan.

| Temperature [°C] | Precursor | Reactive gas | $S_a$ | $S_q$ |
|---|---|---|---|---|
| 200 | DMAI | $H_2O$ | 0.94 | 1.23 |
| 600 | DMAI | $O_2$ | 1.35 | 1.71 |
| 520 | ATI | $N_2$ | 4.79 | 6.09 |

for all deposition temperatures in both atmospheres. The diffraction patterns (Fig. 3) do not show any peaks associated with the formation of a crystalline structure. The absence of significant broad humps, except that of the Si substrate near 69° (c.f. Fig. S1) suggests the formation of amorphous thin film materials. These results are similar to the results of former works using XRD and transmission electron microscopy (TEM) for alumina films grown from DMAI and ATI precursors for temperatures up to 700 °C.[1,4–10,12,14–19]

In the absence of XRD phase identification, we investigated the composition of the films processed from ATI (Fig. 4) and DMAI (Fig. 5–7) using XPS (after systematic erosion of ca. 100 nm surface layer) and EPMA, which allows precise determination of the O/Al ratio using internal standards. The obtained O/Al ratios are compared to the ratios expected for AlOOH and $Al_2O_3$ references. In the case of the films obtained from evaporated ATI (Fig. 4), the composition at temperatures of 420 °C and lower corresponds to that of partially hydroxylated alumina $AlO_{1+x}(OH)_{1-2x}$. At temperatures between 480 and 620 °C, the composition is, however, near that of stoichiometric $Al_2O_3$. For the temperatures from 420 to 620 °C, absolutely no C was detected by XPS. At higher temperature (700 °C), the O/Al ratio decreases to 1.44 while a small concentration of ca. 4 at.-% C is detected by XPS. As shown by the C 1s binding energy (Fig. 4b), this carbon is almost exclusively related to aliphatic moieties, and most likely results from carbon residues of ATI isopropoxide ligands trapped in the film.

Table 2. Typical DLI MOCVD process parameters used during the preparation of alumina thin films using DMAI precursor, cyclohexane solvent and a total pressure of 5 Torr.

| Temperature [°C] | Reactive gas | Injection mixing flow [sccm] | Dilution flow [sccm] | Deposition rate [μm $h^{-1}$] |
|---|---|---|---|---|
| 150 | $H_2O$ | 300 | 300 | 0.4 |
| 200 | $H_2O$ | 300 | 300 | 0.6 |
| 250 | $H_2O$ | 300 | 300 | 1.1 |
| 300 | $H_2O$ | 300 | 300 | 1.8 |
| 500 | $O_2$ | 400 | 400 | 0.3 |
| 600 | $O_2$ | 400 | 400 | 1.2 |
| 600 | $N_2$ | 450 | 400 | 0.9 |
| 700 | $O_2$ | 400 | 400 | 2.5 |

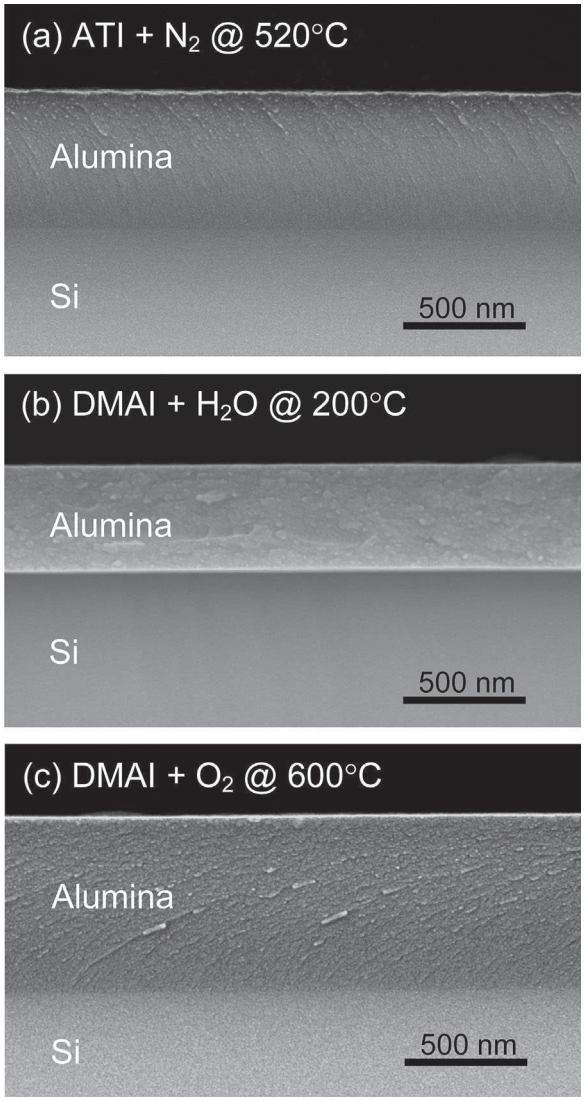


Fig. 2. SEM cross-sections of alumina films deposited onto Si substrates using, a) evaporated ATI in $N_2$ at 520 °C, and b) for films grown by DLI CVD of DMAI at 200 °C in the presence of $H_2O$, and c) at 600 °C in the presence of $O_2$. Film thicknesses are ca. 630, 440, and 720 nm, respectively.

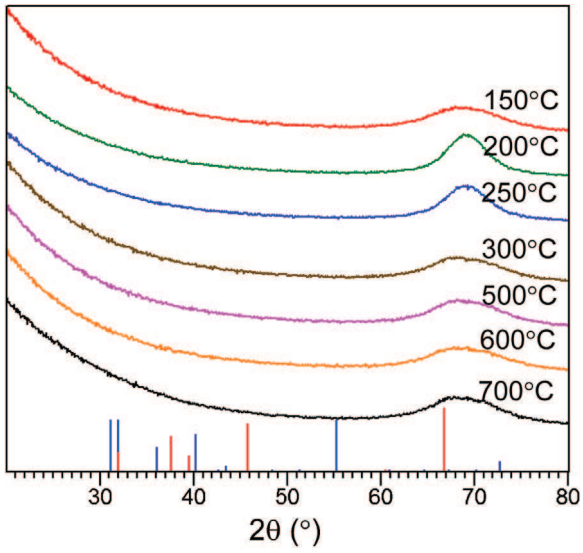


Fig. 3. XRD patterns for alumina thin films deposited in the presence of $H_2O$ for substrate temperatures from 150 to 300 °C and in the presence of $O_2$ for substrate temperatures from 500 to 700 °C. The broad humps around 69° result from the Si substrate in the 3° $\theta$ offset configuration (see Experimental and Fig. S1). Red and blue vertical bars represent the reference patterns of $\gamma$-$Al_2O_3$ and $Al_4C_3$.

The films prepared from DMAI at 150 and 200 °C in the presence of $H_2O$ vapor show O/Al atomic ratios of 1.81 and 1.67, respectively (Fig. 5). These values are between those of AlOOH (2.0) and $Al_2O_3$ (1.5), and correspond to the formation of partially hydroxylated alumina $AlO_{1+x}(OH)_{1-2x}$, as is the case for the materials formed from evaporated ATI at higher temperatures from 360 to 420 °C. The films prepared at 250 and 300 °C show O/Al ratios of 1.54 and 1.50, respectively, in good agreement with the formula $Al_2O_3$. The C content, measured by XPS, is below 1 at.-% for these films and is related to the formation of aliphatic carbon moieties (Fig. 6), as measured for the films grown from evaporated ATI.

The material processed at 500 °C in the presence of $O_2$ has an O/Al ratio of 1.48, which may be ascribed to the formula $Al_2O_3$. The films prepared at 600 and 700 °C have O/Al ratios of 1.25 and 1.10, well below 1.50. Lower temperatures (400 °C for instance) were not feasible since, in these conditions, the deposition rate is extremely small, i.e., lower than the rate of 0.2 μm $h^{-1}$ measured at 500 °C (Table 2). Similar to the film grown from evaporated ATI at 700 °C, the decrease in O/Al ratio is clearly related to an increase in the carbon concentration, up to about 6.5 at.-% in the film prepared at 700 °C. The presence of carbon was also found by Schmidt et al. during the preparation of alumina films from evaporated DMAI in this temperature range.[18,19] In addition to the formation of aliphatic carbon moieties, this result can also suggest the formation of the aluminum carbide $Al_4C_3$ and/or aluminum oxycarbides, e.g., $Al_4O_4C$ or $Al_2OC$,[28–31] along with $Al_2O_3$, to lead to the generic composition of $Al_2O_xC_{3/2-x/2}$. The formation of oxycarbides can be thought to result from the partial substitution of one $C^{4-}$ anion for two $O^{2-}$ anions, leading to the formulae $Al_4O_4C$, $Al_2OC$, and ultimately $Al_4C_3$.

The XPS results for the samples prepared at low temperature in the presence of $H_2O$ vapor are presented in Figure 6. For all samples, the absence of reduced species such as $Al_2O_{3-x}$ and of the metallic Al signals, expected around 73.5 and 72.5 eV, respectively, in Al 2p spectra suggests that ion sputtering erosion did not significantly alter the bulk structure of the alumina material. The amount of aliphatic carbon (C-C and C-H bonds) is less than 1 at.-% for all samples, as observed for the films grown from evaporated ATI. The carbon species are likely to result from the precursor and/or cyclohexane solvent residues incorporated in the film during growth. The Al 2p signal

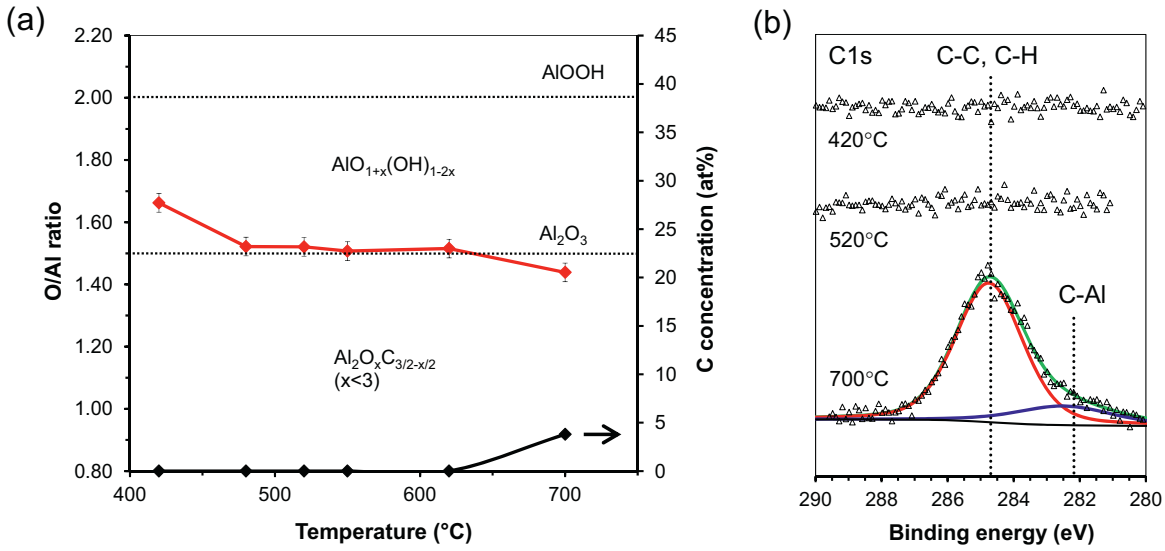


Fig. 4. Elemental composition of alumina films prepared from the sublimation of ATI, using a) EPMA (O/Al atomic ratios; red), and b) high-resolution C 1s XPS (C atomic concentration; black). Films were deposited in the presence of $N_2$ from 420 to 700 °C. Each sample was measured with EPMA four to twelve times in various locations to check the homogeneity of the composition. The decomposition of the XPS spectra into the assigned chemical species is shown for each core level.

around 74.4 eV apparently shows a single symmetric peak. Its main contribution is from $Al^{3+}$ in an $O^{2-}$ framework. A small proportion overlapping with the main peak (not shown) is thought to result from Al oxyhydroxides, for which the response is expected to be very similar to that of the oxide. Indeed, the signals for Al 2p in $Al_2O_3$, AlOOH, and $Al(OH)_3$ are very close in binding energy and hard to separate.[32–34] The O 1s signal is a much better discriminant for the presence of hydroxyl groups, which have a peak expected at about 1.3 eV offset from the main $O^{2-}$ peak of $Al_2O_3$.[33,34] Indeed, the measured O 1s signals clearly show a main peak around 531.4 eV at the location expected for $O^{2-}$ in the $Al_2O_3$ framework,[32,33,35,36] accompanied by a shoulder of increasing intensity with decreasing temperature around 532.7 eV, attributable to hydroxyl groups. The relative amount of hydroxyl groups increases as the temperature decreases, in very good agreement with the increasing O/Al ratio measured with EPMA (Fig. 5). In summary, the results for films processed at low temperature in the presence of $H_2O$ show the quasi-absence of carbon and the presence of hydroxyl groups for the lowest deposition temperatures whereas no hydroxyls are detected at 300 °C, in good agreement with the EPMA results.

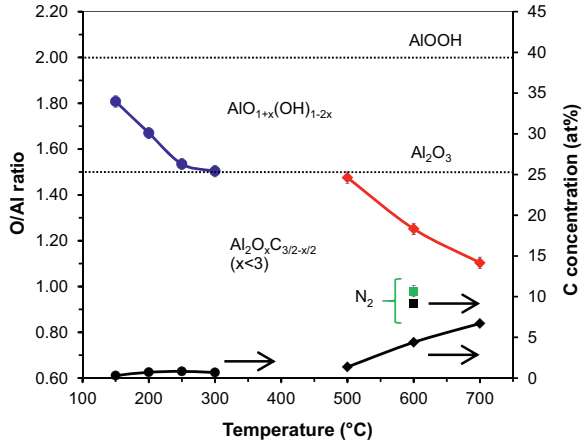


Fig. 5. Elemental composition of the alumina films prepared from the DLI CVD of DMAI, using EPMA (O/Al atomic ratios; blue for $H_2O$, red for $O_2$, and green for $N_2$) and XPS (C atomic concentration; black). Films were deposited in the presence of $H_2O$ from 150 to 300 °C (circles), in the presence of $O_2$ from 500 to 700 °C (diamonds) or in the presence of $N_2$ only at 600 °C (squares). Each sample was measured with EPMA four to six times in various locations to check the homogeneity of the composition.

The XPS results for samples prepared at high temperature in the presence of $O_2$ are presented in Figure 7. The Al 2p and O 1s signals clearly show the presence of intensity at the locations expected for $Al_2O_3$ with an Al 2p binding energy of about 74.4 eV and O 1s binding energy near 531.5 eV, as discussed above. Moreover, the signals observed at about 73.2 eV in Al 2p and near 282.0 eV in C 1s were previously attributed to aluminum carbide $Al_4C_3$.[37,38] The relative atomic contribution of carbon in aluminum (oxy) carbide over aliphatic carbon is 75% at 500 °C, 60% at 600 °C and 73% at 700 °C, and the absolute amount of carbon bonded to Al clearly increases with increasing deposition temperature from about 1 at.-% at 500 °C to about 5 at.-% at 700 °C. This result is in agreement with a former report, showing that the CVD from TMA and $CH_4$ leads to pure $Al_4C_3$ films only at temperatures as high as 1150 °C.[30] Here, the presence of aluminum (oxy) carbides could be the result of the reaction of cyclohexane solvent with the growing alumina film. This is suggested by earlier results that showed the absence of C in films grown at 560 °C during the MOCVD of DMAI in pure $O_2$.[7] Other

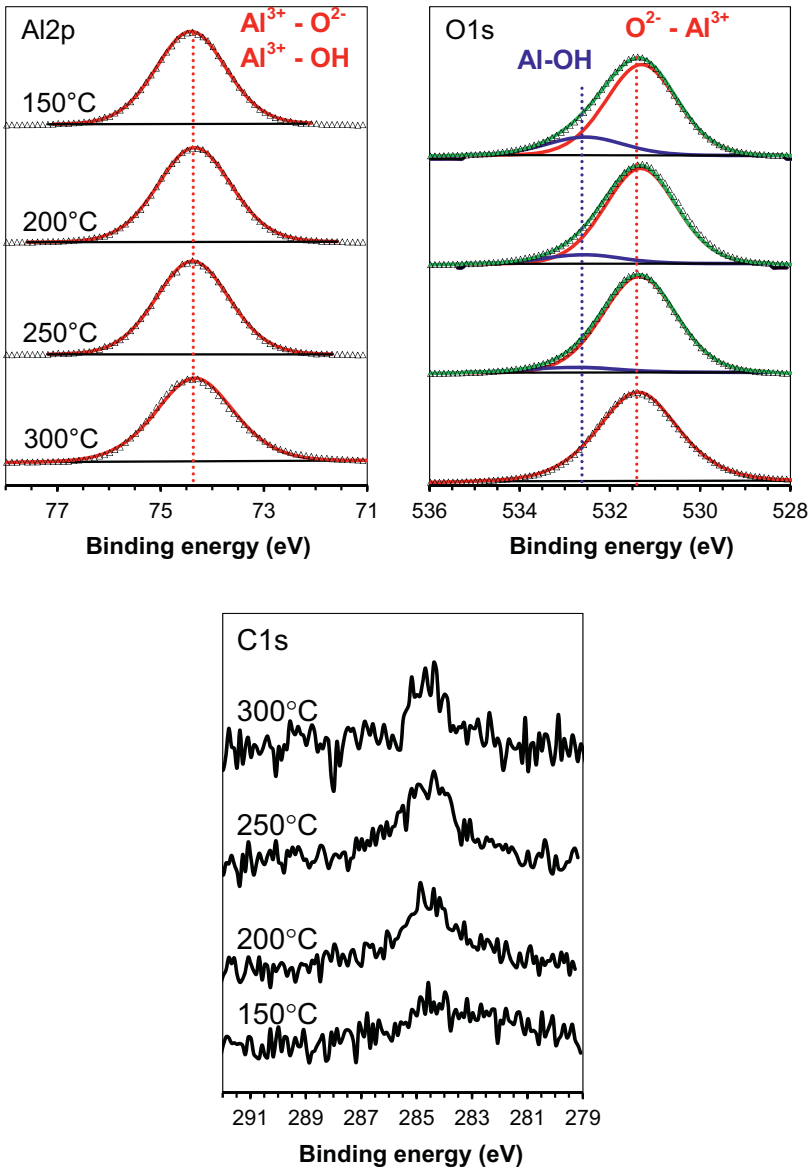


Fig. 6. High-resolution XPS images (Al 2p, O 1s, and C 1s) of alumina films deposited from 150 to 300 °C in the presence of $H_2O$. The decomposition of the Al 2p and O 1s spectra into the assigned chemical species is shown for each core level. The intensities of the C 1s signals correspond to less than 1 at.-%, see Figure 5.

reports, however, showed that substantial amounts of C were incorporated into alumina films when using a DMAI precursor in pure $N_2$ atmosphere.[17,18] This contrasts with the results of films grown from evaporated ATI for which very little C and no (oxy) carbide are measured (Fig. 4). DMAI is composed of two C atoms linked to Al, and can, by itself, be expected to partly contribute to the formation of (oxy) carbides. It is interesting to note that a film processed at 600 °C in pure $N_2$ (no $O_2$ added) had a significantly higher C concentration (9.2 at.-%), with about 75% in the form of aluminum (oxy) carbides, concomitant with a much lower O/Al ratio (0.98) than for samples deposited in a $N_2/O_2$ atmosphere (Fig. 5). This result indicates the positive role of $O_2$ in reducing the amount of formed oxycarbides, as suggested by the earlier work of Barecca et al.[7]

In summary, the results show that the DLI CVD process of DMAI leads to the formation of partially hydroxylated films at low temperatures (<250 °C) in the presence of $H_2O$. This is somewhat analogous to what is obtained for the process using evaporated ATI in $N_2$ at temperatures below 480 °C. At higher temperatures, the films are stoichiometric in both cases. Moreover, in the presence of $O_2$, the DLI CVD of DMAI leads to the formation of aluminum oxide at 500 °C, and mixed oxycarbides at 600 °C and above. The formed aluminum (oxy) carbides originate either from the precursor, or from the interaction between the precursor and solvent molecules. As suggested by earlier reports, a larger $O_2$/DMAI ratio may lead to fully stoichiometric alumina films at higher temperatures.[7] Conversely, decreasing the $O_2$/DMAI ratio, or using only pure $N_2$

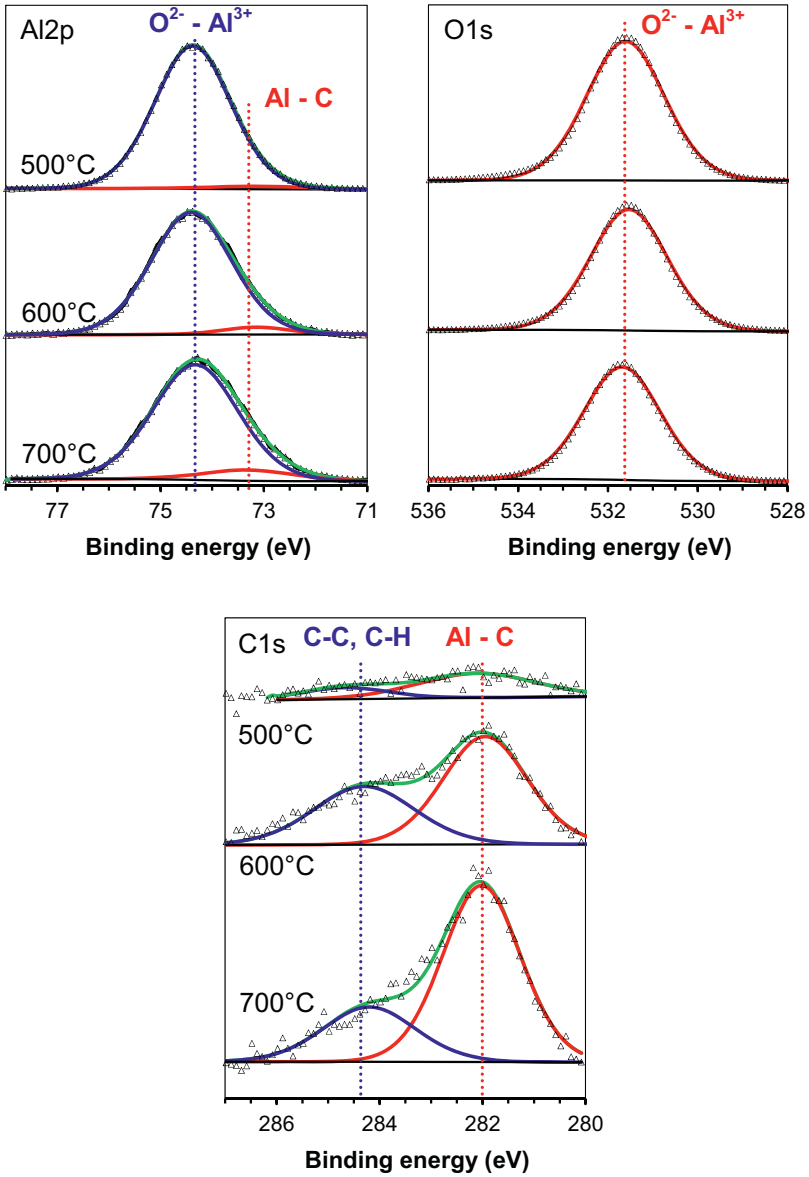


Fig. 7. High-resolution XPS images (Al 2p, C 1s and O 1s) of alumina thin films deposited from 500 to 700 °C in the presence of $O_2$. The decomposition of the spectra into the assigned chemical species is shown for each core level.

(Fig. 5.[17–19]), can lead to the formation of oxycarbides at 600 °C and above. Tuning the $O_2$/DMAI ratio thereby opens a route for the preparation of aluminum oxycarbide films with new properties (optical, mechanical, etc.). On the other hand, if the aim is to prepare stoichiometric alumina films to act as oxidation barriers, it is necessary to use an $O_2$ source in large concentration or to employ $H_2O$ vapor as an efficient co-reactant to avoid the formation of (oxy) carbides.

## 3. Conclusion

DLI CVD of alumina thin films from DMAI precursor has been investigated for the first time. $O_2$ and $H_2O$ oxygenating environments, have been used to assist in the formation of $Al_2O_3$. The produced films are extremely smooth ($R_a$ in the range 1–2 nm) and have an amorphous structure. The composition of the films evolves from a partial oxyhydroxide $AlO_{1+x}(OH)_{1-2x}$ to $Al_2O_3$ for films processed at low temperatures (150–300 °C) in the presence of $H_2O$. The films prepared at higher temperatures (500–700 °C) in the presence of $O_2$, consist of the oxide $Al_2O_3$, either pure (500 °C) or mixed with aluminum (oxy) carbide (600 and 700 °C). The amount of (oxy) carbides is found to increase with the increase in temperature, as well as with the decrease of the $O_2$/DMAI ratio. The use of CVD can make the processes applicable to complex-in-shape materials. Future work will be devoted to characterizing the oxidation barrier properties of these films for the protection

of alloys in the aeronautics industry, in particular light polymer composites and Mg alloys requiring maximum processing temperatures not exceeding 200 °C.

## 4. Experimental

*Thin Film Preparation*: Thin films were prepared using a home-made horizontal hot-wall CVD reactor equipped with various gas lines and mass flow controllers (MFC), injection and bubbling systems, and a quartz tube (25 mm diameter, 300 mm length) heated by a resistive furnace (Fig. S2). A dry pump and pressure gauges connected to the output of the quartz tube were used to keep the total reaction pressure at 5 Torr. Silicon samples (10 mm × 10 mm) cut from 4″ Si(001) wafers (Sil'tronix) were placed on a stainless steel holder in the center of the quartz tube where the temperature was uniform. Gas lines and the evaporation steel chamber of the DLI system were heated to ca. 80 °C or 130 °C to prevent the condensation of DMAI and ATI precursors, respectively. The DLI system (Kemstream) consists of a set of two injectors, one connected to a $N_2$ pressurized Schlenk flask for liquid injection in the mixing chamber, and one connected to a $N_2$ pressurized line for gas mixing of the solution droplet with $N_2$ and transfer to the evaporation chamber. The precursor solution was prepared in a Schlenk flask inside a glovebox circulated with purified Ar (99.9997%, Air Products) by adding a known amount of DMAI solution (>99%, Air Liquide) into the flask. The sealed flask was taken out of the glovebox and completed with the appropriate quantity of anhydrous cyclohexane (99.5%, $H_2O$ < 10 ppm, Sigma-Aldrich) using an air-tight, Ar purged, glass syringe to prepare a solution of 0.2 M DMAI. Then, the Schlenk flask was connected to the gas line and to the liquid injector inlet, and was purged several times with pressurized $N_2$ (99.9999%, Praxair). The frequency and opening times of the injection system were controlled to feed the evaporation chamber with small precursor solution droplets mixed with $N_2$ gas with a mixing $N_2$ flow set from 300 to 450 sccm. For the low temperature process, 120 sccm of $N_2$ bubbling through deionized $H_2O$ (>20 MΩ cm) kept at room temperature was added to the reactor via another gas line. For the high temperature process, 50 sccm of $O_2$ (99.9995%, Air Products) was added to the $N_2$ dilution gas (300–400 sccm). In both cases, the oxidants were in large excess compared to DMAI. For the process using evaporation of ATI in a super-cooled, molten state, the preparation was identical to that reported elsewhere using the bubbler filled with ATI heated to a temperature of 90 °C.[10–12] Growth conditions for both the low and high temperature processes using DMAI are listed in Table 2.

*Materials Characterization*: The film thickness was measured using optical reflectivity (Mikropack, Nanocalc 2000). Thickness was confirmed by measuring the film thickness in SEM cross-sections. Surface morphology and roughness of the samples were measured using SEM and AFM. SEM images were taken in backscattered mode on a JEOL JSM-7800F field emission SEM operated at 10 kV. Samples measured with SEM were fractured then covered by a thin layer of sputtered platinum to prevent charging effects. AFM was used in ambient conditions on an Agilent Technologies 5500. Scanning was performed in contact mode with tips of spring constant of about 0.292 N m$^{-1}$ (AppNano). Scanning rate was set to 2 μm s$^{-1}$. Images were processed with the software Pico Image (Agilent Technologies). The film crystalline structure was measured by XRD on a Bruker D8 Advance using a Cu Kα (1.5418 Å) X-ray tube operated at 40 kV and 40 mA, a Ni filter, and solid-state Lynxeye detector in $\theta+3°/\theta-3°$ configuration. Samples were measured on a zero background holder and a $\theta$ offset of 3° was applied between the X-ray source and detector arms to suppress the strong (004) diffraction of the samples on the Si substrates, normally measured around 69° (Fig. S1). EPMA was used to accurately determine the O/Al ratios in the films. Characterization was conducted with a Cameca SXFive apparatus operated at 10 and 15 keV and calibrated using a high purity alumina standard. Samples were covered by a thin layer of carbon inside an evaporation chamber (Leica) to prevent charging effects. Each sample was measured four to twelve times in various locations to determine the spatial homogeneity of the sample composition.

XPS measurements were performed on a Thermo Scientific K-Alpha instrument using monochromatic Al Kα (1486.6 eV) capable of a base pressure of $10^{-9}$ Torr or less, and equipped with a detector positioned at 90° with respect to the sample surface. The spectrometer energy calibration was performed using the Au $4f_{7/2}$ (83.9 ± 0.1 eV) and Cu $2p_{3/2}$ (932.7 ± 0.1 eV) photoelectron lines. Charging compensation and neutralization were applied by using a dual beam flood gun. The probed areas were about 400 μm in diameter. A survey scan was collected before and after surface erosion to measure the composition and check for possible contaminants. Surface erosion was employed using Ar ions accelerated at 2 kV, resulting in an erosion rate of about 0.08 nm s$^{-1}$. Constant pass energy of 30 eV and energy steps of 0.1 eV were used for high resolution scans. The energy scale was fixed by setting the adventitious carbon C 1s energy to 284.4 eV. The photoelectron peaks were analyzed by Gaussian/Lorentzian (G/L = 70/30) peak fitting and using a Shirley background. The atomic concentrations were determined from photoelectron peak areas using the atomic sensitivity factors reported by Scofield, taking into account the transmission function of the analyzer. This function was calculated at different pass energies from Ag 3d and Ag MNN peaks collected for a silver reference sample. C concentrations, reported from these quantifications, are estimated to be exact within ±20%.

Received: September 15, 2015
Revised: October 8, 2015

[1] S. Blittersdorf, N. Bahlawane, K. Kohse-Höinghaus, B. Atakan, J. Müller, *Chem. Vap. Deposition* **2003**, *9*, 194.
[2] V. A. C. Haanappel, H. D. van Corbach, R. Hofman, R. W. J. Morssinkhof, T. Fransen, P. J. Gellings, *High Temp. Mater. Processes* **1996**, *15*, 245.
[3] S. S. Yom, W. N. Kang, Y. S. Yoon, J. I. Lee, D. J. Choi, T. W. Kim, K. Y. Seo, P. H. Hur, C. Y. Kim, *Thin Solid Films* **1992**, *213*, 72.
[4] A.-M. Lazar, W. P. Yespica, S. Marcelin, N. Pébère, D. Samélor, C. Tendero, C. Vahlas, *Corros. Sci.* **2014**, *81*, 125.
[5] S. Krumdieck, S. Davies, C. M. Bishop, T. Kemmitt, J. V. Kennedy, *Surf. Coat. Technol.* **2013**, *230*, 208.
[6] F. Wiest, V. Capodieci, O. Blank, M. Gutsche, J. Schulze, I. Eisele, J. Matusche, U. I. Schmidt, *Thin Solid Films* **2006**, *496*, 240.
[7] D. Barecca, G. A. Battiston, R. Gerbasi, E. Tondello, *J. Mater. Chem.* **2000**, *10*, 2127.
[8] G. A. Battiston, R. Gerbasi, *Chem. Vap. Deposition* **2002**, *8*, 193.
[9] Y. Balcaen, N. Radutoiu, J. Alexis, J.-D. Beguin, L. Lacroix, D. Samélor, C. Vahlas, *Surf. Coat. Technol.* **2011**, *206*, 1684.
[10] M.-M. Sovar, D. Samélor, A. N. Gleizes, C. Vahlas, *Surf. Coat. Technol.* **2007**, *201*, 9159.
[11] A. N. Gleizes, C. Vahlas, M.-M. Sovar, D. Samélor, M.-C. Lafont, *Chem. Vap. Deposition* **2007**, *13*, 23.
[12] V. Sarou-Kanian, A. N. Gleizes, P. Florian, D. Samélor, D. Massiot, C. Vahlas, *J. Phys. Chem. C* **2013**, *117*, 21965.
[13] Y.-I. Ogita, N. Saito, *Thin Solid Films* **2015**, *575*, 47.
[14] X. Liu, S. H. Chan, F. Wub, Y. Li, S. Keller, J. S. Speck, U. K. Mishra, *J. Cryst. Growth* **2004**, *408*, 78.
[15] W. Koh, S.-J. Ku, Y. Kim, *Thin Solid Films* **1997**, *304*, 222.
[16] S. Y. Lee, B. Luo, Y. Sun, J. M. White, Y. Kim, *Appl. Surf. Sci.* **2004**, *222*, 234.
[17] G. Carta, M. Casarin, N. El Habra, M. Natali, G. Rossetto, C. Sada, E. Tondello, P. Zanella, *Electrochim. Acta* **2005**, *50*, 4592.
[18] B. W. Schmidt, B. R. Rogers, W. J. Sweet III, C. K. Gren, T. P. Hanusa, *J. Eur. Ceram. Soc.* **2010**, *30*, 2301.
[19] B. W. Schmidt, B. R. Rogers, C. K. Gren, T. P. Hanusa, *Thin Solid Films* **2010**, *518*, 3658.
[20] S. S. Lee, E.-S. Lee, S. H. Kim, B. K. Lee, S. J. Jeong, J. H. Hwang, C. G. Kim, T.-M. Chung, K.-S. An, *Bull. Korean Chem. Soc.* **2012**, *33*, 2207.
[21] W. Cho, K. Sung, K.-S. An, S. S. Lee, T.-M. Chung, Y. Kim, *J. Vac. Sci. Technol. A* **2003**, *21*, 1366.
[22] S. E. Potts, G. Dingemans, C. Lachaud, W. M. M. Kessels, *J. Vac. Sci. Technol. A* **2012**, *30*, 021505.
[23] Y. Wu, S. E. Potts, P. M. Hermkens, H. C. M. Knoops, F. Roozeboom, W. M. M. Kessels, *Chem. Mater.* **2013**, *25*, 4619.
[24] J. Yang, B. S. Eller, M. Kaur, R. J. Nemanich, *J. Vac. Sci. Technol. A* **2014**, *32*, 021514.
[25] T. B. Jackson, A. C. Hurford, S. L. Bruner, R. A. Cutler, in *Silicon Carbide* (Eds. J. W. Cawley, C. Semler), The American Ceramic Society, Columbus USA **1989**, p. 227.
[26] L. Baggetto, J. Esvan, C. Charvillat, D. Samélor, H. Vergnes, B. Caussat, A. Gleizes, C. Vahlas, *Phys. Status Solidi* **2015**, *12*, 989.
[27] M. Manin, S. Thollon, F. Emieux, G. Berthome, M. Pons, H. Guillon, *Surf. Coat. Technol.* **2005**, *200*, 1424.
[28] L. M. Foster, G. Long, M. S. Hunter, *J. Am. Ceram. Soc.* **1956**, *39*, 1.
[29] J. M. Lihrmann, T. Zambetakis, M. Daire, *J. Am. Ceram. Soc.* **1989**, *72*, 1704.
[30] Y. Ozcatalbas, *Compos. Sci. Technol.* **2003**, *63*, 53.
[31] D. Kima, Y. Onishi, R. Oki, S. Sakai, *Thin Solid Films* **2014**, *557*, 216.

[32] H. He, K. Alberti, T. L. Barr, J. Klinowski, *J. Phys. Chem*. **1993**, *97*, 13703.
[33] A. Hess, E. Kemnitz, A. Lippitz, W. E. S. Unger, D.-H. Menz, *J. Catalysis* **1994**, *148*, 270.
[34] J. T. Kloprogge, L. V. Duong, B. J. Wood, R. L. Frost, *J. Colloid Interface Sci*. **2006**, *296*, 572.
[35] S. Verdier, L. El Ouatani, R. Dedryvère, F. Bonhomme, P. Biensan, D. Gonbeau, *J. Electrochem. Soc*. **2007**, *154*, A1088.
[36] L. Baggetto, N. J. Dudney, G. M. Veith, *Electrochim. Acta* **2013**, *90*, 135.
[37] R. Hauert, J. Patscheider, M. Tobler, R. Zehringer, *Surf. Sci*. **1993**, *292*, 121.
[38] B. Maruyama, F. S. Ohuchi, *J. Mater. Res*. **1991**, *6*, 1131.